ADVANCED HEALTHCARE MATERIALS
www.advhealthmat.de

Developing MiR-133a Zipper Nanoparticles for Targeted Enhancement of Thermogenic Adipocyte Generation

*Sang Ah Yi, Thanapat Pongkulapa, Sarah Nevins, Li Ling Goldston, Meizi Chen, and Ki-Bum Lee**

Existing delivery methods for RNAi therapeutics encounter challenges, including stability, specificity, and off-target effects, which restrict their clinical effectiveness. In this study, a novel miR-133a zipper nanoparticle (NP) system that integrates miRNA zipper technology with rolling circle transcription (RCT) to achieve targeted delivery and specific regulation of miR-133a in adipocytes, is presented. This innovative approach can greatly enhance the delivery and release of miR-133a zippers, increasing the expression of thermogenic genes and mitochondrial biogenesis. he miR-133a zipper NP is utilized for the delivery of miRNA zipper-blocking miR-133a, an endogenous inhibitor of Prdm16 expression, to enhance the thermogenic activity of adipocytes by modulating their transcriptional program. Inhibition of miR-133a through the miR-133a zipper NP leads to more significant upregulation of thermogenic gene expression (*Prdm16* and *Ucp1*) than with the free miR-133a zipper strand. Furthermore, miR-133a zipper NPs increase the number of mitochondria and induce heat production, reducing the size of 3D adipose spheroids. In short, this study emphasizes the role of RNA NPs in improving RNAi stability and specificity and paves the way for broader applications in gene therapy. Moreover, this research represents a significant advancement in RNAi-based treatments, pointing toward a promising direction for future therapeutic strategies.

1. Introduction

Therapeutic approaches that utilize ribonucleic acid (RNA) moieties have shown significant promise in addressing a broad spectrum of diseases and health conditions, from viral infections and genetic abnormalities to numerous cancer types.[1,2] The pivotal role of RNA in a myriad of vital biological processes highlights its potential as a therapeutic agent. It is instrumental in gene expression and the synthesis of proteins. In contrast to DNA-based therapies, RNA's regulation of cellular processes is transient, thereby positioning it as a promising approach for drug development in clinical environments. Furthermore, DNA-based therapeutics may carry a risk of genotoxicity due to the possibility of off-target mutations in the genome, a concern not as prevalent in RNA-based approaches.[3] In contrast, RNA-focused therapies can interact with biological processes by manipulating RNA, effectively addressing the fundamental issues present in various diseases. This approach enables the correction of molecular dysfunctions, offering a targeted therapeutic strategy for addressing various medical conditions. For instance, 17 RNA technologies have received clinical approval for therapeutic purposes.[4] Besides these approved technologies, 222 distinct RNA technologies are undergoing clinical trials.[4] These include antisense oligonucleotides (ASOs), microRNA (miRNA) mimics, messenger RNAs (mRNAs), small interfering RNAs (siRNAs), and aptamers.

While RNA interference (RNAi) therapeutics hold significant promise, the practical clinical application of these treatments hinges on the ability to deliver RNA to cells and tissues in a targeted and efficient manner. It is crucial to ensure that RNA drugs are accurately directed to their intended locations within the body to harness the full therapeutic potential of this promising technology. Various strategies, including viral vectors, liposomes, polymers, and nanoparticles (NPs), have been developed for delivering siRNA into cells.[2,5] These methods utilize different materials for cell uptake and incorporate extended templates capable of carrying multiple siRNAs. This enhances the therapeutic potential and quantity of siRNA delivered. However, conventional RNAi technology with current delivery methods faces challenges, such as agent instability, limited therapeutic efficacy, and potential off-target effects. For example, small RNA silencing technologies such as miRNA inhibitors and siRNA have been correlated with off-target gene expression, which can be reduced but

S. A. Yi, T. Pongkulapa, S. Nevins, L. L. Goldston, M. Chen, K.-B. Lee
Department of Chemistry and Chemical Biology
Rutgers
The State University of New Jersey
123 Bevier Road, Piscataway, NJ 08854, USA
E-mail: kblee@rutgers.edu
S. A. Yi
Chemical Biology Program
Memorial Sloan Kettering Cancer Center
New York, NY 10065, USA
The ORCID identification number(s) for the author(s) of this article can be found under https://doi.org/10.1002/adhm.202400654

DOI: 10.1002/adhm.202400654

not eliminated through chemical modifications such as a 2′-*O*-methyl ribosyl substitution at position 2 from the 5′ end in the antisense strand.[6,7] Modified nucleic acid strategies, such as locked nucleic acids (LNAs) connected between 2′-O and 4′-C,[8] miRNA sponges,[9] and miRNA masks,[10] have also been developed to increase the specificity of these RNAi therapeutics. Furthermore, adeno-associated virus (AAV) and lipid nanoparticle (LNP) formulations have recently been used to transfect RNA therapeutics and vaccines, including for delivering COVID-19 vaccines, as they assist in RNA uptake into cells.[11,12] However, a main issue with the AAV-mediated delivery system is off-target effects such as vaccine-induced immune thrombotic thrombocytopenia (VITT).[13,14] It has been reported that the AAV shell and proteins can recruit platelets to surround foreign proteins, which induces abnormal blood clotting.[14,15] In addition, polyethylene glycol (PEG), a common component of LNPs, is thought to cause severe allergic reactions, including anaphylaxis, upon vaccination.[16]

The aforementioned challenges underscore the imperative need for advanced delivery methods to maximize the efficacy of RNA-based therapies. Consequently, there is an urgent need for an innovative platform capable of delivering small RNAs with high precision and minimal side effects aimed at either inhibiting or replicating natural nucleic acids. RNA-based NP technologies show promise in surmounting the limitations of traditional RNA therapeutics, including low loading capacity, brief molecular half-life, and unintended off-target effects.[5,17–19] Moreover, they can also be functionalized by targeting ligands for directed delivery to specific cells or tissues. This makes NPs an ideal vehicle for delivering RNA therapeutics. Initial self-assembled RNA particle design by Lee et al. showed the potential of RNA self-assembly into NPs.[20] Subsequently, RNA NPs have been confined to smaller sizes and had template modification to deliver multiple siRNA at once.[18,21] In short, RNA-based NP technologies have the potential to revolutionize the treatment of many diseases, such as cancer, genetic disorders, and infectious diseases. NP-based methods offer the potential to deliver various types of RNA biomolecules. An example is the miRNA zipper, developed by Meng et al., which has demonstrated enhanced efficacy in miRNA silencing.[22] The zipper system inhibits the action of endogenous oligonucleotides through end-to-end connection to form a zipper structure with the target, therefore silencing its detrimental effect.[22] This system potentially advances current RNAi technology by creating miRNA zipper NPs for the enhanced silencing of miRNAs critical to disease onset. For example, utilizing the miRNA zipper design has great potential for inhibiting miR-133a, a critical miRNA target for controlling adipocyte cell remodeling through regulation of the thermogenic gene expression pathway.[23,24] These advancements might revolutionize the development of RNAi-based therapeutics for various diseases.

One area of particular interest is the study and manipulation of adipocytes, which play a crucial role in energy balance and metabolism. Adipocytes store surplus energy as lipid droplets, thereby preventing fat accumulation in other tissues and protecting them from lipotoxicity.[25] Understanding and potentially altering the function of these cells through RNAi could provide novel insights into energy expenditure, involving processes such as the activation of brown fat or the transformation of white fat into brown-like fat.[26] This approach is especially relevant given the distinct ways in which different types of adipocytes, such as white and brown adipocytes, store energy in lipid droplets.[27] Brown adipocytes have a larger surface area, facilitating easier energy utilization in the form of lipids.[27] Additionally, it is worth noting that heat generation can induce energy expenditure.[27] For this purpose, miR-133a is a critical barrier to adipocyte browning by directly targeting the 3′ UTR on Prdm16, a key transcription factor for thermogenic gene expression. Prdm16 directs Myf5-positive progenitor cells with bidirectional cell fates, muscle cells, and brown adipocytes toward a brown fat lineage.[28] There are two types of brown fat cells – innate brown adipocytes and inducible brown-like fat cells or beige adipocytes. Brown adipose differentiation is promoted through ectopic PRDM16 expression in myoblasts, activating brown fat-selective transcriptional programing.[28,29] More importantly, forced PRDM16 expression in white fat depots triggers the formation of beige adipocytes with increased thermogenic gene expression, including UCP1.[30,31] UCP1-enriched adipocytes can consume stored lipids through non-shivering heat generation,[32] so the phenotypic changes promoted in inducible beige adipocytes through thermogenic gene expression would be desirable for effectively treating obesity and related metabolic complications.

Hence, miR-133a inhibition or depletion, which induces PRDM16, has been investigated as a browning strategy. Preventing PRDM16 suppression through the transfection of anti-miR-133[24] or knockout of miR-133a.[33] resulted in adipocyte browning of subcutaneous adipose tissues. Our earlier study identified that reducing miR-133a levels with a small molecule promotes the browning of white adipose tissues and exhibits anti-obesity effects.[34] Excess lipid accumulation in vivo causes the expansion of adipose tissues through an increase in either adipocyte number (hyperplasia) or size (hypertrophy).[35,36] Hyperplasia occurs with angiogenesis and prevents the onset of insulin resistance, while hypertrophic expansion of adipocytes results in inflammation, fibrosis, and hypoxia and is linked to a decrease in angiogenesis.[35–37] Furthermore, hypertrophic adipocyte remodeling in obesity increases the likelihood of developing metabolic disorders by altering the adipokine secretome and inducing insulin resistance.[38] Adipocyte remodeling into thermogenic adipocytes can help circumvent the harmful effects of excessive body fat accumulation to improve metabolic status.[38] As a result, the inhibition of miR-133a holds great potential in promoting adipocyte remodeling and serving as an essential therapeutic strategy for obesity treatment.

To advance miRNA-based therapies and address critical challenges related to obesity treatment, herein we developed a novel hybrid miR-133a zipper NP system that induces the browning of white adipocytes effectively and selectively, as depicted in **Figure 1A**. This innovative, bio-inspired NP design can suppress specific endogenous or targeted miRNAs through a miRNA zipper mechanism. Additionally, it can deliver siRNA together with miRNA, thus enhancing the therapeutic potential of the system (Figure 1A).

In the context of T7 RNA polymerase activity, we used rolling circle transcription (RCT) with circular DNA (cDNA) templates. These templates contained the miR-133a zipper and GFP siRNA sequences, which formed self-assembling NPs (Figure 1B). We confirmed that these NPs were uptaken by cells and processed by intracellular dicer to simultaneously release miR-133a zippers

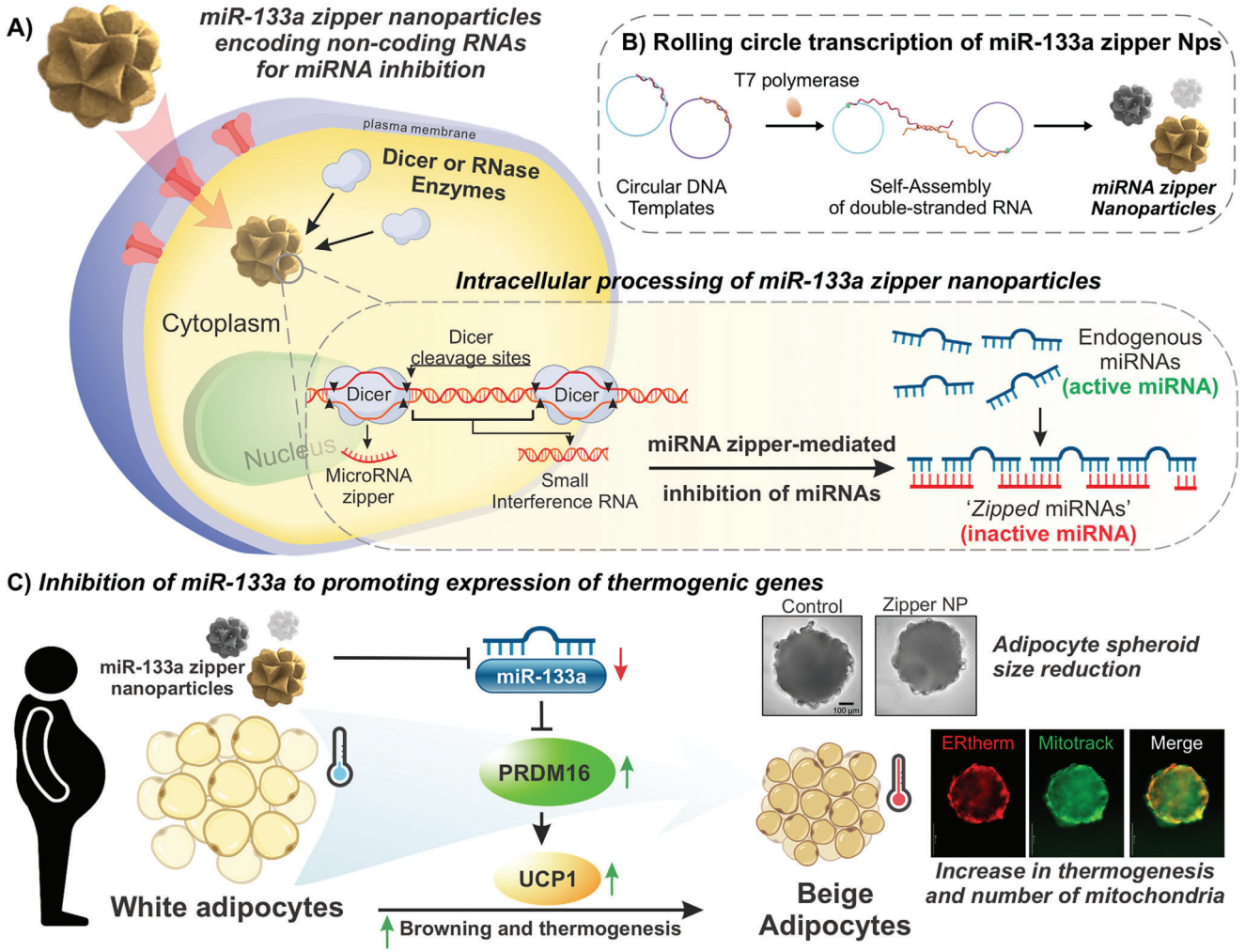

Figure 1. MiR-133a zipper NP-mediated miRNA inhibition of miR-133a and induction of beige adipocytes. A) Schematic illustration of miR-133a zipper NPs encoding miRNA zipper for intracellular miRNA inhibition via complementary interaction. B) Fabrication process of miR-133a zipper NPs via RCT. C) MiR-133a zipper NPs inhibit miRNA-133a, resulting in upregulation of thermogenic genes (i.e., PRDM16, UCP1), hence increasing mitochondrial biogenesis and thermogenesis in adipocytes.

to inhibit miR-133a and siRNA targeting GFP for gene silencing. We assessed the significant effects of the miR-133a zipper-releasing NPs on thermogenic gene expression and mitochondrial biogenesis in adipocytes. The miR-133a zipper showed better inhibition of miR-133a compared to other inhibitory sequences, as evidenced by its stronger binding capacity and therapeutic effectiveness. Moreover, the treatment of 3D adipose spheroids with the miR-133a zipper NP system resulted in a decrease in adipose tissue size and an increase in thermogenesis, suggesting the potential of the system for the treatment of obesity (Figure 1C). Moreover, we confirmed that the template strand was cleaved by dicer to release multiple RNA sequences and that the NP was taken up by cells, which was achieved by incorporating a siRNA sequence for GFP-silencing into the miR-133a zipper NP. Overall, our innovative hybrid miR-133a zipper NP system not only enhances the efficiency of the miR zipper through NP-based delivery, but also demonstrates the possibility of delivering multimodal RNAi therapeutics altogether, highlighting its wide range of potential applications in biomedicine.

2. Results and Discussion

2.1. Design, Synthesis, and Characterization of miRNA Zipper NPs

DNA strands were carefully designed to enable the creation of DNA templates capable of transcription and self-assembly into a repeated bubble-like RNA secondary structure. This specific structure is essential for the successful formation of the NPs. To this end, two linear single-stranded DNA templates encompassing the sequence for the miR-133a zipper and either the sense or antisense GFP siRNA underwent T4 ligation for cDNA template formation, followed by in vitro transcription using T7 polymerase for miR-133a zipper NP fabrication (**Figure 2A**). As the dicer-induced cleavage of long double-stranded RNAs preferentially occurs within 21–23 nucleotides from the overhang,[39] the complimentary duplex region had 21 nucleotides for releasing miR-133a zipper from the NP without junk nucleotides (Figure S1, Supporting Information). Based on an earlier study,[22] the

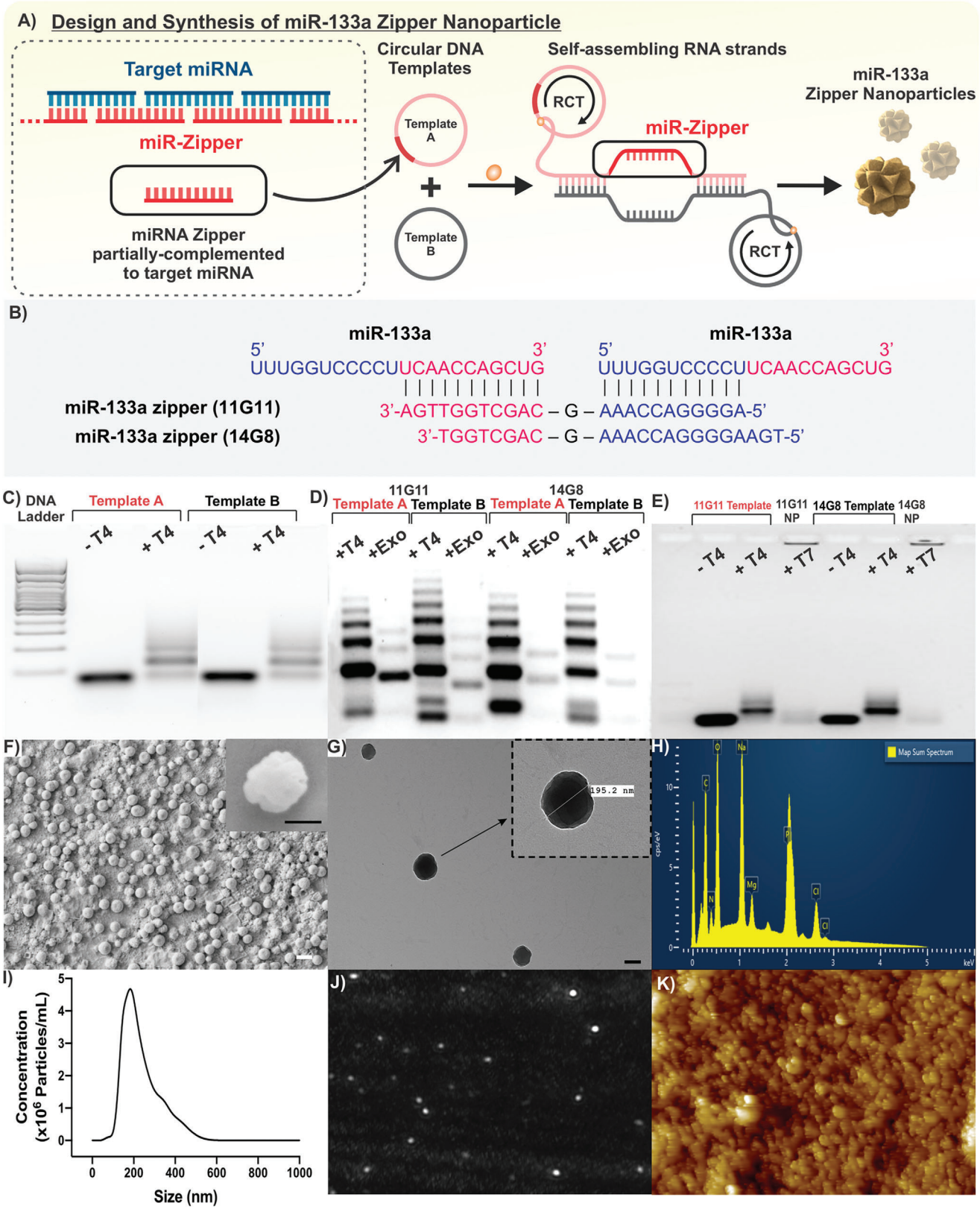

Figure 2. Synthesis and characterization of miR-133a zipper NPs. A) Schematic diagram of miR-133a zipper NP fabrication process via template circularization, followed by RCT. B) miR-133a zipper designs used in this study, namely 11G11 and 14G8. Refer to Figure S2 (Supporting Information) for full-size gel. C) Confirmation of template circularization after ligation. (M = 100 bp ladder, +T4 = ligation reaction in the presence of T4 ligase,

miR-133a zipper sequences were designed to have the 5′ and 3′ regions of miR-133a, in which the two sides of the zipper are reversely linked with one gap nucleotide in the structure. Therefore, the 5′ and 3′ sides of the miR-133a zipper can bind to part of the miR-133a target sequence through a complementary interaction (Figure 2B).

We generated two miR-133a zipper sequence designs with varying 5′ and 3′ arm lengths (11G11, same length of arms, 14G8, longer 5′ arm) to determine the most effective zipper sequence (Figure 2B). The designed miR-133a zipper sequence includes a G base gap between the sequences binding each portion of the miRNA because of the need for a base gap for efficient binding, as well as the presence of an AAA repeat in miR-133a sequence which could prevent proper binding with an A base gap. Following the process of cDNA formation, the transformation from a linear to a circular conformation of the DNA structure resulted in a decrease in migration rate during gel electrophoresis. This is because cDNA moves slower than linear DNA in native PAGE, primarily due to its bulky shape.[40] Therefore, a slower migration of cDNA compared to linear DNA confirmed the successful formation of the circular template (Figure 2C). Exonucleases 1 and 3 were used to degrade improperly formed cDNA, as a more uniform template led to better NP formation, ensuring that the starting template was fully formed cDNA (Figure 2D; Figure S2, Supporting Information). The cDNA templates formed through T4 ligation were subsequently utilized for RCT with T7 polymerase to generate miR-133a zipper NPs (Figure 2E; Figure S2, Supporting Information).

The size and surface morphology of the as-synthesized miR-133a zipper NPs was confirmed by scanning electron microscope (SEM) and transmission electron microscope (TEM). The SEM images revealed the spherical shape of the particles with the surface roughness, which is consistent with RNA NPs observed from literature using similar synthetic methods (Figure 2F).[20,41–44] The SEM and TEM images showed the NPs had a size ≈200 nm (Figure 2F,G). Batch-to-batch variation was tested with DLS, and no significant size difference was observed across the three batches. The average hydrodynamic size of all three batches was 279.73 nm, with a standard deviation of 16.37 nm. (Figure S3, Supporting Information). Furthermore, the NPs have a low average polydispersity index across three batches at 0.144 with a standard deviation of 0.045 (Figure S3, Supporting Information). The elemental composition of the NPs was analyzed using energy-dispersive X-ray spectroscopy (EDS), which verified the presence of carbon, oxygen, phosphorus, and nitrogen, as well as a trace amount of $Mg2^{+}$ ions, confirming the successful incorporation of the designed components into the NP structure. Mg^{2+} ions have been shown to help limit siRNA degradation by stabilizing RNA tertiary structure (Figure 2H; Figure S4, Supporting Information).[45,46] $MgCl_2$ is a reaction buffer component used for cDNA formation and NP synthesis, and a small amount was incorporated into the NP during synthesis. Furthermore, Mg^{2+} has been shown to promote cell entry and endosomal escape through Mg^{2+} ion interactions with the lipid bilayer.[17,45] Nanoparticle Tracking Analysis (NTA) assay confirmed the homogeneity of miR-133a zipper NPs (Figure 2I,J). The particles were monodispersed, with the majority population at a size of 174.4 nm and a mean size of 236.9 nm. Atomic force microscopy (AFM) was also used to elucidate the morphology and surface of the NPs (Figure 2K), compared to previously reported miRNA-inhibiting technologies. Moreover, we inserted the zipper seq.

2.2. Optimization of miRNA-133a Zippers for Effective Inhibition

RNAi-based therapy has become a critical therapeutic approach, including a variety of forms allowing for diverse treatment options. RNAi therapeutics aims to regulate diverse cellular physiology at the post-transcriptional level by silencing a natural process of gene silencing. A previous study showed that reversine, a small molecule first developed by Peter G. Schultz group,[47] promotes white adipocyte browning through miR-133a suppression.[34] However, small molecule-based therapies can induce adverse effects because small molecules have an array of targets rather than a specified target, miR-133a in this case. Hence, the miRNA zipper design is optimal for silencing miR-133a to minimize off-target effects. Our hybrid miR-133a zipper NP structure contains an alternating sequence of the fully-hybridized duplex region made of siRNA targeting green fluorescent protein (GFP) and a non-hybridized open region of the miR-133a zipper (bubble region), which are released after cleavage by intracellular dicer or RNases. (**Figure 3**A).

First, we compared target miRNA binding efficiency to evaluate small RNA binding after release from the self-assembled NP and RNA interference. To confirm miRNA zipper formation and compare the binding efficiency of the miR-133a zipper original oligomer, LNA-containing oligomer, zipper NP, and the 5′ → 3′ miRNA sequence outside of cells, binding to the target sequence was determined using a gel electrophoresis RNA binding shift assay with native polyacrylamide gel electrophoresis (PAGE). LNA is another tool for increasing the stability and affinity of oligonucleotides, such as miR-133a zipper, and exhibits a bicyclic structure in which a 2′-O-CH_2-4′ linkage makes a flexible furanose more rigid and resistant to nuclease[8,48] (Figure S5, Supporting Information). Based on evidence that oligonucleotides containing LNA in both ends of the miRNA sequence inhibit mRNA expression efficiently,[48] we designed miR-133a zipper (11G11) to contain LNA at both 3′ and 5′ ends while minimizing self-complementarity (Figure S5, Supporting Information).

The quantification of both the disappearance of the miR-133a target sequence and the appearance of the bound target was conducted to assess the binding efficiency (Figure 3B,C; Figures

-T4 = ligation reaction in the absence of T4 ligase). Refer to Figure S2 (Supporting Information) for full-size gel. D) Confirmation of exonuclease 1 and 3 digestion after template circularization (+Exo = Exonuclease 1 and 3). Refer to Figure S2 (Supporting Information) for full-size gel. E) Confirmation of miR-133a zipper NP formation. Refer to Figure S2 (Supporting Information) for full-size gel. F) Scanning electron microscope (SEM) image of miR-133a zipper NPs (scale bar = 2μm), inset: high magnification SEM image of miR-133a zipper NPs (scale bar = 100nm). G) Transmission electron microscope (TEM) image of miR-133a zipper NP (scale bar = 100 nm), inset: higher magnification TEM image of RNA NP. H) Elemental composition of siRNA NPs I) NP concentration and size from NP Tracking Analysis (NTA). J) NTA video and K) AFM image of miR-133a zipper NPs (image is 10 μm by 8.33 μm).

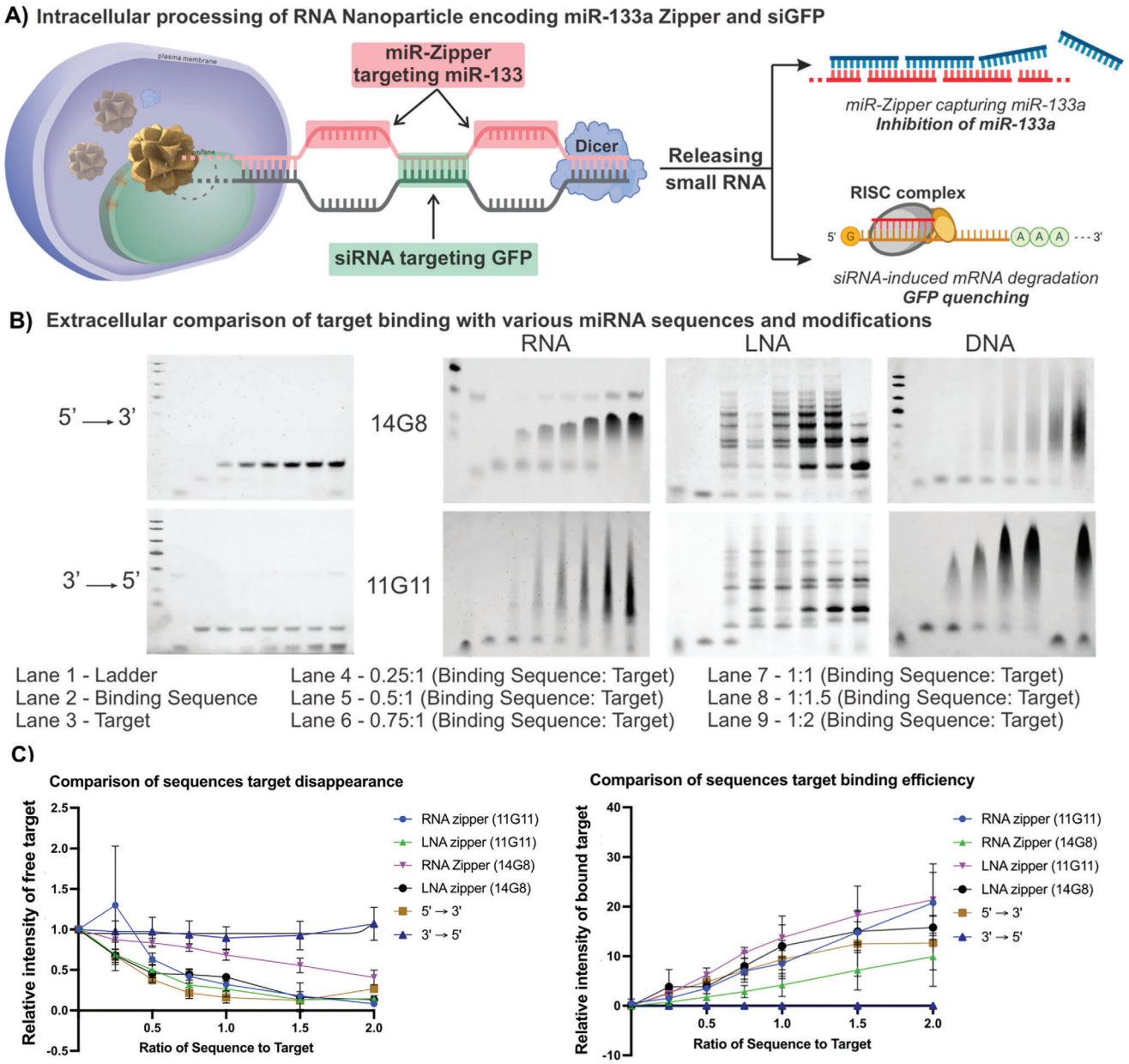

Figure 3. Functional confirmation of released small RNAs from miR-133a zipper NP. A) Schematic illustration of miR-133a zipper NP system encoding both single-stranded RNA zipper complementary to miR-133a and double-stranded siRNA complementary to GFP mRNA for simultaneous gene inhibition. B) Images of native PAGE gels to test RNA binding to target. Refer to Figures S6, S8, and S10 (Supporting Information) for Full-size gels. C) Quantification of RNA binding to target and target sequence disappearance relative to the intensity of the fully unbound target from gels (n=3). Refer to Figures S6, S8, and S10 (Supporting Information) for Full-size gel triplicates.

S6, S8, and S10, Supporting Information). Throughout all the lanes, the target weight was held steady, whereas the weight of each binding oligonucleotide was progressively raised, reaching a maximum of twice the target weight. Therefore, the amount of each sequence that binds the miRNA target could be quantified relative to the free sequence and target. The miR-133a zipper sequences, 11G11 and 14G8, had superior binding to the standard 5′ → 3′ miRNA sequence, based on analysis of the gels for RNA binding kinetics (Figures S7, S9, and S11, Supporting Information). This can be correlated with the inability of the complete miRNA complement to bind more than a single miR-133a target sequence. Thus, the 5′ → 3′ miRNA sequence stopped showing an increase in bound product past a 1 to 1 ratio of the target to its complementary sequence. The binding efficiency of the zipper sequence, including LNA, was similar for 11G11 miRNA zipper and slightly higher than the 14G8 miRNA zipper (Figures S7, S9, and S11, Supporting Information). The efficient binding to the target miRNA sequence outside of cells is critical for the optimal effectiveness of the miR-133a zipper NP. The exponential increase in band intensity at various lengths with the addition of

higher RNA, DNA, and LNA-based zipper oligonucleotides to target ratios can be correlated with the formation of different-length zippers. The 3′ → 5′ miRNA sequence showed no significant binding at any ratio to the target sequence, further illustrating the inefficiencies of standard complementary sequences for RNA binding. The comparable binding of the RNA zipper sequence to the ssDNA sequence gives evidence that the ssDNA template used for RNA transcription is optimal for RNA zipper sequence and NP development. Furthermore, we confirmed an increase in binding efficiency with a G base gap over an A base gap, which we chose for miR-133a zipper NP formation due to sequence structure, as previously discussed (Figures S12 and S13, Supporting Information).

2.3. Targeted Delivery and Intracellular Release of miR-133a Zipper NP in Adipocytes

Next, we assessed intracellular delivery of the miR-133a zipper NPs by tracking the fluorescence signal of 6-carboxyfluorescein (FAM)-containing miR-133a zipper NPs in adipocytes differentiated from 3T3-L1 preadipocyte cells (**Figure 4A**). The FAM signal was detected near the nucleus of adipocytes 4 h after NP treatment and overlapped with the nuclear membrane after 8 h (Figure 4B). The data indicates that bubble-structured miR-133a zipper NPs are delivered into the nucleus of adipocytes within 8 h. To verify the release of miRNA zipper and siRNA from the miR-133a zipper NP, native PAGE was run after a dicer cleavage assay, which enabled us to quantify the amount of miRNA zipper released from the NPs over time (Figure 4C; Figure S14, Supporting Information). We then used RT-qPCR to quantify the amount of miRNA using standard curve quantification. The result shows that the RNA zipper accounted for 8.9% wt. of the miR-133a zipper NP (Figure S15, Supporting Information). The theoretical amount of zipper in the particle would be 12.9% showing the quantified amount is close to the theoretical amount. Furthermore, based on the 8.9% by weight, 10 nM LNA should deliver the same weight of the miR-133a zipper as 7.36 μg mL^{-1}, 30 nM LNA is equiv. to 20 μg mL^{-1} miR-133a zipper NP, and 50 nM LNA is equiv. to 36.7 μg mL^{-1} miR-133a zipper NP. GFP-signal quenching was studied in GFP-expressing adipocytes upon GFP-siRNA release from the miR-133a zipper NP to confirm intracellular cleavage of the small RNA (Figure 4D). At 24 and 48 h after treatment of adipocytes with the NP, GFP signal intensity was remarkably ablated by siRNA release regardless of miR-133a zipper design (Figure 4D). The numbers of cells expressing GFP were counted and normalized to the number of DAPI-stained cells. This further confirmed a significant decrease in GFP-expressing cells upon miR-133a zipper NP treatment (Figure 4E).

miR-133a directly interacts with *Prdm16* mRNA transcript to act as an endogenous suppressor of the expression of *Prdm16* gene.[24] Therefore, deleting or antagonizing miR-133a successfully elevated thermogenic gene expression in adipose tissues and browning of mouse adipose tissues.[24,33] In our strategy, after miR-133a zipper NP delivery to adipocytes and cleavage by intracellular RNase, the released miR-133a zippers would freely bind to the miR-133a target, resulting in the induction of Prdm16-mediated thermogenesis. To assess the stable delivery of the miR-133a zipper with the miR-133a zipper NP and determine therapeutic potential, changes in expression levels for key downstream targets of miR-133a were compared after miR-133a zipper NP delivery or the transfection of miRNA zipper oligonucleotides and LNA-based zipper oligonucleotides, which were designed as illustrated in Figure S5 (Supporting Information). The cell viability was tested after delivery of the miR-133a zipper NP or LNA with Lipofectamine, a widely used transfection reagent for in vitro experiments, in a concentration-dependent manner to check cell viability after NP delivery in comparison to control adipocytes and LNA delivered with Lipofectamine (Figure S16, Supporting Information). To evaluate the therapeutic effects of both the LNA zipper and the RNA NP, the same amount of LNA and miR-133a zipper NPs were delivered by weight based on the percentage of miR-133a zipper experimentally determined to be in the NP. To further confirm the therapeutic effects of both the LNA zipper and the RNA NP the same concentrations were tested to confirm RNA expression 24 h after NP delivery. A significant increase in PRDM16 and UCP1 expression was observed with the NP in a concentration dependent manner (Figure S17, Supporting Information). No significant increase was seen in UCP1 with LNA zipper and the PRDM16 upregulation had less significance with LNA zipper than the miR-133a zipper NP. To compare the functional effects of three different compounds, namely the miR-133a zipper original oligomer, LNA-containing oligomer, and NP, expression levels for *Prdm16* and its downstream thermogenic gene, *Ucp1* were tested (Figure 4F). Lipofectamine was used to deliver either the standard zipper sequence or the LNA sequence at a concentration of 50 nM. Notably, the *Prdm16* and *Ucp1* transcription levels were the highest in adipocytes treated with the miR-133a zipper NP at 20 μg mL^{-1} (Figure 4G). However, mature white adipocyte marker (*Fabp4*) gene expression was not significantly altered by all three developed miR-133a zipper delivery systems, meaning a consistent differentiation rate of white fat-like cells, although the cells displayed browning characteristics with NP delivery (Figure 4G).

Enhancing oligonucleotide therapeutic intracellular stability has been a critical challenge. Therefore, researchers have studied nucleotide backbone modification as a tool to enhance the stability and affinity of oligonucleotide drugs.[49] LNA is one of the most favorable RNA modifications for RNA therapeutics due to significant improvements in RNA-binding affinity and stability.[48] The first group to suggest the miRNA zipper concept utilized LNA to enhance the zipper oligonucleotide stability and affinity for binding.[22] Nevertheless, our self-assembled NP was more potent than LNA-containing miR-133a zipper. It has been reported that LNA inclusion showed a larger effect on short oligomer (less than 10 bases) binding than longer oligomer binding.[50] Since miRNA and siRNA are usually 21–23 nucleotides in length,[1] our approach to deliver RNAi as a nanostructure is more suitable for RNAi therapeutics than LNA inclusion. Our data suggests that transfection with nascent zipper strands has minimal impact even after prolonged exposure. The RNA design includes double-stranded siRNA segments surrounding the miRNA zipper sequence, creating a more resistant nanostructure to enzymatic degradation. In comparison, single-stranded RNA is more susceptible to enzymatic hydrolysis and is less stable in blood plasma.[20] The improved stability within cells leads to a stronger therapeutic effect, even though the RNA zipper and the LNA zipper sequence have similar

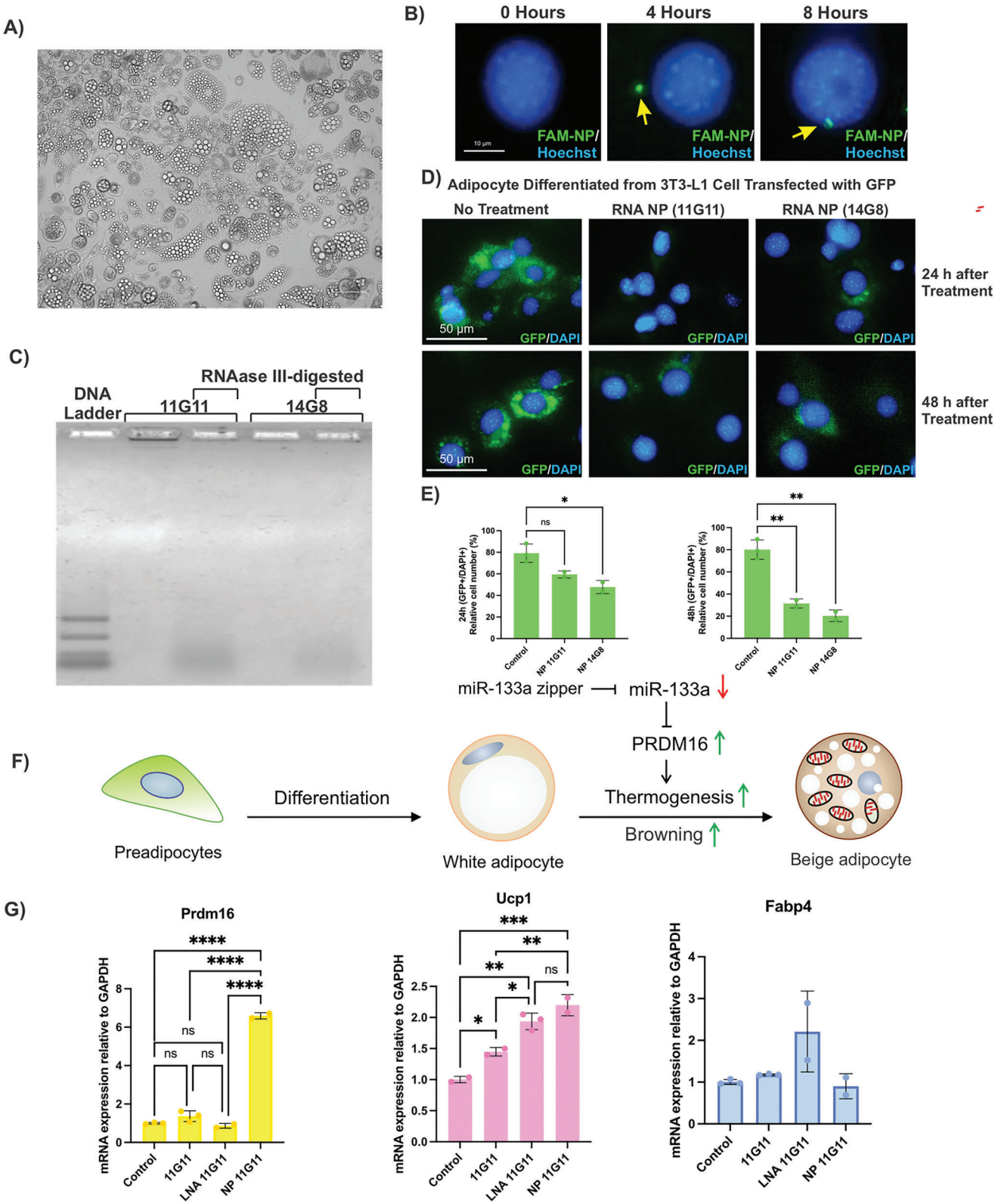

Figure 4. Effects of miR-133a zipper NP delivery systems on thermogenic gene expression. A) Brightfield image of differentiated 3T3-L1 adipocytes (scale bar = 100 μm) B) Fluorescent images showing the cellular uptake of 11G11 miR-133a zipper NPs in a 3T3-L1 adipocyte (Green = fluorescein-labeled RNA NPs, Blue = nucleus staining by Hoechst 33342). C) The release of miRNA zipper from miR-133a zipper NPs in Dicer reactions. Refer to Figure S14 (Supporting Information) for Full-size gels. D) GFP knockdown by miR-133a zipper NPs after 24 and 48 h of transfection (scale bar = 50μm). E) Quantification of GFP-positive 3T3-L1 adipocytes after treatment of miR-133a zipper. A one-way ANOVA with post-hoc Tukey test (n = 2-3, *p < 0.05,

efficiencies in binding targets in extracellular environments. NP stability during intracellular delivery may be further linked to the presence of Mg^{2+} ions, which have been shown to stabilize RNA tertiary structure, preventing degradation of the RNA before cellular delivery and cleavage by dicer.[45,46] Therefore, the intracellular delivery rate of miR-133a zipper NP may be higher than nascent oligonucleotides due to its high stability in biological conditions, leading to significant differences in miR-133a zipper effectiveness in cells, although the binding efficiency to the target extracellularly is similar. Thus, the assembly of miR-133a zipper into the NP likely allowed for more significant changes in gene expression than LNA due to the enhanced uptake into cells. Future research that compares the cellular uptake efficiency between LNA and miR-133a zipper NP could determine if the observed increase in gene expression changes in vitro is mainly caused by improved cellular uptake.

2.4. MiR-133a Zipper NP Induces Thermogenic Remodeling of Adipocytes

Next, we investigated the influence of the miR-133a zipper sequence on miRNA inhibitory action using 11G11 and 14G8 miR-133a zipper sequences for NP formation. RT-qPCR data showed that both the 11G11 and the 14G8 miR-133a zipper NPs highly enhanced thermogenic gene expression, while transfection with Lipofectamine of original 11G11 and 14G8 miR-133a strands showed minimal effects (**Figure** 5A). Interestingly, there was no significant difference in effects between the 11G11 and 14G8 zipper sequences when self-assembled into the NP (Figure 5A). Similarly, Prdm16 and Ucp1 protein levels were elevated upon 11G11 and 14G8 NP treatment, as shown with a western blot assay (Figure 5B; Figure S18, Supporting Information). To assess the targeted binding capability of the miR-133a zipper NP, we conducted qPCR analysis to evaluate the levels of miR-133a in adipocytes (Figure S19, Supporting Information). The knockdown efficiency of miR-133a was ≈50–60% for both NPs, while the transfection of original strands or LNA-containing zipper strands did not significantly reduce miR-133a levels (Figure S19, Supporting Information). The data showed that miR-133a zipper NPs can effectively decrease miR-133a intracellular levels, thus preventing miR-133a-mediated Prdm16 suppression.

UCP1 mediates non-shivering thermogenesis by converting electrochemical energy into heat in the inner mitochondrial membrane.[51] Thermogenic activation in adipocytes is frequently accompanied by mitochondrial biogenesis, a hallmark of brown fat.[52] Thus, we tested whether the miR-133a zipper NP induces mitochondrial biogenesis in adipocytes. Mitochondrial contents were evaluated with MitoTracker Green staining dye, which stains mitochondria in live cells. A strong green fluorescence signal should be detected in thermogenic beige or brown-like adipocytes containing a high density of mitochondria, while a number of low mitochondria should lead to a weak green signal in non-thermogenic white adipocytes (Figure 5C). The green fluorescence signal intensity showed a significant increase, as anticipated, when the miR-133a zippers (11G11 or 14G8) were released by the NPs (Figure 5D). However, the increase in signal intensity was minimal when each original strand was transfected individually (Figure 5D). Quantification analysis of the mitotracker signal relative to Hoechst 33342 staining the nucleus also showed clear mitochondrial biogenesis by miR-133a zipper NPs (Figure 5E). The signal intensities in cells transfected with the original zipper strands showed a slight increase, yet remained lower than in cells transfected with the NP, aligning with the unchanged thermogenic gene expression. Collectively, the data presented in Figure 5 demonstrates that both designs of the miR-133a zipper NP, 11G11 and 14G8, effectively promote the thermogenic activation of adipocytes.

2.5. MiR-133a Zipper NP Reduces the Size of 3D Adipose Spheroids Through Thermogenesis

Three-dimensional (3D) adipose spheroids are optimal to recapitulate the morphology and function of in vivo adipose tissues in fat depots.[53] To assess the impact of the miR-133a zipper NP on reducing adipose size, we closely observed the changes in the size of 3D adipose spheroids following the administration of these NPs. Initially grown as a monolayer on the surface of plates, adipocytes were detached and re-aggregated within a 3D culture system. The resulting adipose spheroids were treated with miR-133a zipper NPs or transfected with the original zipper strands on alternate days. 6 days after the initial treatment, the spheroid size was monitored, and RNA was extracted for an RT-qPCR assay (**Figure** 6A). Using FAM-tagged miR-133a zipper NPs, we observed NP delivery into the 3D adipose spheroids (Figure S13, Supporting Information). Both miR-133a zipper NPs, 11G11 and 14G8, caused a significant reduction in the diameter of adipose spheroids starting on day 4, while original zipper strands had little effect on adipose spheroid size, even on day 6 (Figure 6B; Figures S20 and S21, Supporting Information). Furthermore, 14G8 miR-133a zipper NPs led to a more significant decrease in spheroid diameter on day 4 than 11G11 miR-133a zipper NPs, although both NPs had similar significance. The theoretical volume of the spheroids based on the spheroid diameter also shows a decrease from the control (Figure S22, Supporting Information). The ratio of the theoretical volume of the spheroid to that of the control demonstrates consistent effects, maintaining a ratio below 1 without significant changes between days 4 and 6 (Figure S23, Supporting Information). Similarly, *Prdm16* and *Ucp1* expression levels were significantly promoted by the zipper system but not by the original strands (Figure 6C).

Since the expansion of adipose tissue is a key hallmark of obesity, inhibiting adipose tissue growth is a critical parameter in assessing the efficacy of therapeutic interventions to treat obesity. Recent studies illustrate that a 3D culture system of adipocytes is a drug-responsive model that can largely replace animal models.[54,55] Therefore, we assessed the mitochondrial biogenesis and thermogenesis of adipose spheroids for functional validation using two bio-tracker dyes that detect mitochondria and

**p < 0.01). F) Schematic illustration of thermogenic beige adipocyte generation from white adipocyte, induced by miR-133a zipper. G) Relative mRNA expression of key thermogenic genes upon treatment of adipocytes with different forms of miR-133a zipper. A one-way ANOVA with a post-hoc Tukey test (n = 2-3, *p < 0.05, **p < 0.01, ****p < 0.0001).

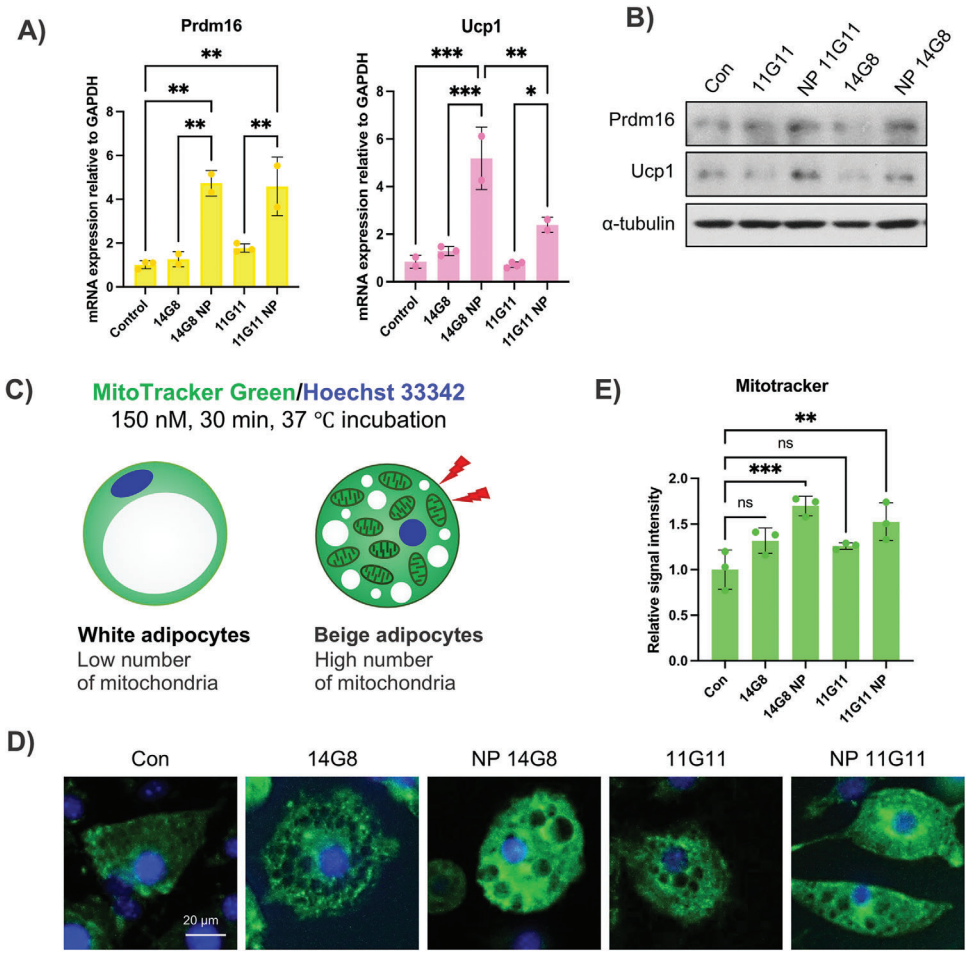

Figure 5. MiR-133a zipper NP induces thermogenic remodeling of adipocytes. A) Relative mRNA expression of key thermogenic genes after treatment of adipocytes with miR-133a zippers. A one-way ANOVA with a post-hoc Tukey test (n=2-3, *p < 0.05, **p < 0.01, ***p < 0.001, ****p < 0.0001). B) Western blot analysis of thermogenic factors after treatment of adipocytes with miR-133a zippers. Refer to Figure S18 (Supporting Information) for full-size gel. C) Evaluation of mitochondrial biogenesis using MitoTracker Green staining. D) Fluorescence microscopic images of adipocytes stained for mitochondrial membrane (green) and nucleus (blue). E) Quantification of MitoTracker-stained cells, presented as relative intensity normalized to Hoechst signal. A one-way ANOVA with a post-hoc Tukey test (n = 3, *p < 0.05, **p < 0.01, ***p < 0.001, ****p < 0.0001).

cellular temperature, respectively (Figure 6D). Upon mitochondrial biogenesis in thermogenically active adipocytes, the green fluorescent signal increased as measured by MitoTracker Green dye fluorescence, while the red fluorescence signal of ERthermAC dye diminished at high temperatures in thermogenic adipocytes (Figure 6E). After exposure to NPs or the original miR-133a zipper strands for 6 days, the adipose spheroids were simultaneously stained with MitoTracker Green and ERthermAC. As expected, green signals indicative of the mitochondria were significantly increased, and red signals were quenched upon 14G8 or 11G11 miR-133a zipper NP treatment (Figure 6F). These signal alterations were also observed in spheroids transfected with the original zipper oligonucleotides, although it was not statistically significant for MitoTracker and led to a less significant increase in thermogenesis than either NP (Figure 6F). The experimental data with 3D adipose spheroids described above indicates that our miR-133a zipper NP can promote thermogenesis and reduce adipose size in tissue-like 3D structural conditions of the cells, confirming the browning effects of miR-133a zipper NP.

The comparability in miR-133a zipper NP effectiveness across different cell models points toward the potential of the NP's ability to create consistent changes to gene expression, an essential factor in RNA therapeutics. Furthermore, considering that miR-133a zipper NPs effectively reduced adipose spheroid size, it is expected that our NPs could reduce adipose mass in clinical use to treat obesity. When we use this ex vivo 3D culture system, we cannot exclude the possibility that only the cells located on the surface of spheroids are affected by the miR-133a zipper. However, vasculature formation occurs throughout adipose tissues in physiological conditions, so miR-133a zipper NP should theoretically be delivered into the inner mass of adipose tissues due to vasculature in vivo conditions. Furthermore, scavenger receptor B1, previously shown to enhance uptake in spheroids, may also play a significant role in the uptake of NPs into adipocytes, as suggested by prior research.[56] Future studies with an adipose spheroid model, including vasculature, and studying NP interactions with scavenger receptor B1 might allow for assessing the delivery and biological effects of nanostructured RNA mimicking

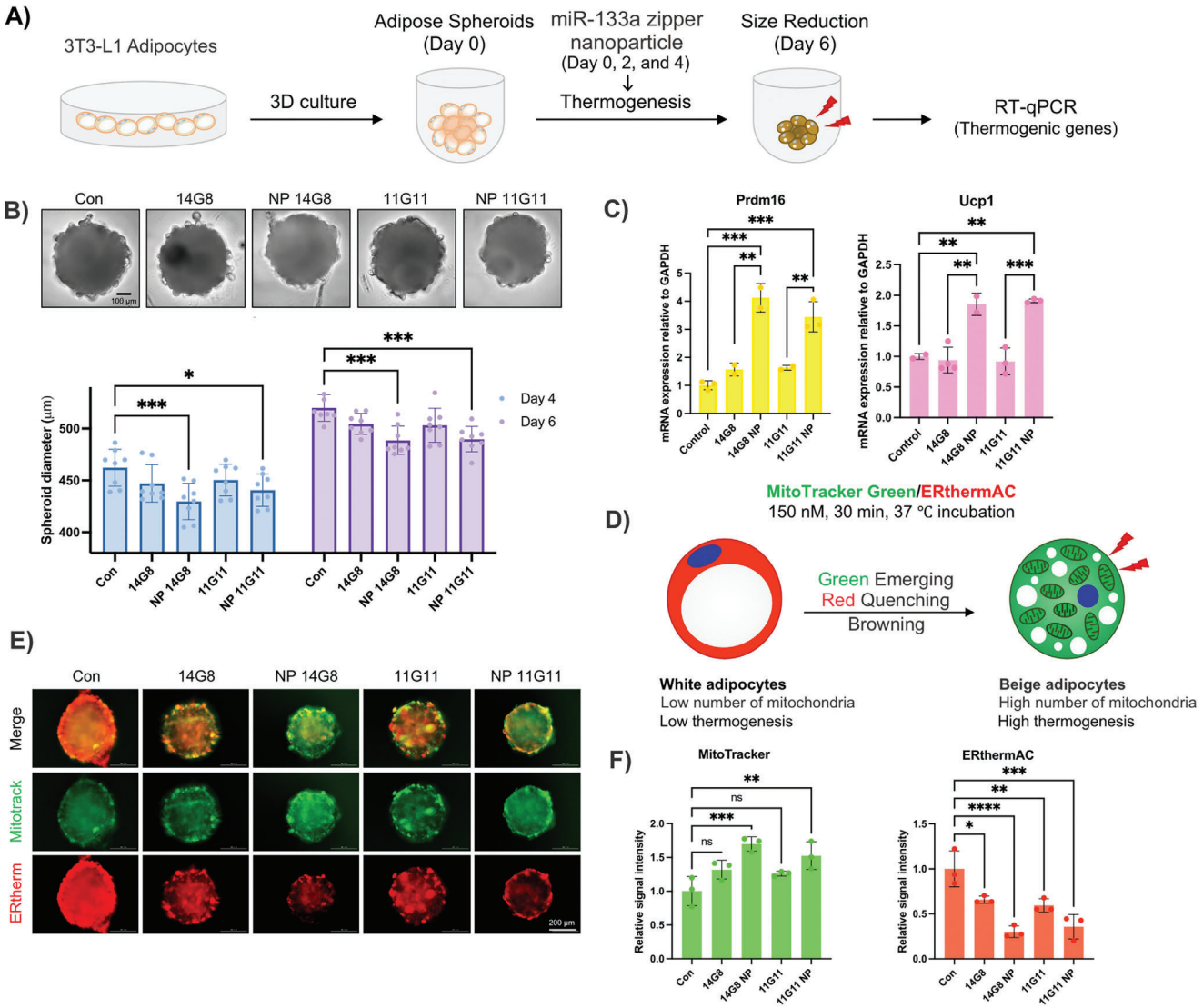

Figure 6. Reduction of adipose mass, and induction of thermogenesis and mitochondria biogenesis in adipose spheroids through miR-133a zipper NP. A) Schematic illustration of experimental workflow for evaluation of thermogenic remodeling in 3T3-L1 adipose spheroids. B) Optical microscopic images and size measurement of adipose spheroids upon treatment with different forms of miR-133a zippers (image scale bar = 100 μm). A two-way ANOVA with a post-hoc Tukey test (n = 8, *p < 0.05, **p < 0.01, ***p < 0.001, ****p < 0.0001). C) Relative mRNA expression level of thermogenic genes from adipocyte spheroids treated with different forms of miR-133a zippers. A one-way ANOVA with post-hoc Tukey test (n = 2-3, *p < 0.05, **p < 0.01, ***p < 0.001, ****p < 0.0001). D) Schematic illustration of experimental workflow for evaluation of thermogenic remodeling in adipose spheroids. E) Representative fluorescent images of adipocyte spheroids stained for mitochondrial membrane (using MitoTracker Green staining [Green]) and thermogenesis (using ERthermAC staining [Red]) after treatment with different miR-133a zippers (scale bar = 200 μm). F) Quantification of fluorescent intensities of mitochondrial membrane and thermogenesis staining from treated adipose spheroids relative to the control. A one-way ANOVA with a post-hoc Tukey test (n = 3, *p < 0.05, **p < 0.01, ***p < 0.001, ****p < 0.0001).

the human body condition. Furthermore, in vivo studies would allow for the study of NP biodistribution, although the NP effect should be limited outside of adipocytes, as previously discussed.

3. Conclusion

While many oligonucleotide delivery platforms for targeted gene therapy have been developed,[49] achieving RNAi delivery with high affinity, specificity, and stability remains a complex challenge. In this study, we have introduced an innovative miRNA-modulating tool that enhances affinity, specificity, and stability by integrating miRNA zipper technology and RCT-based RNA NP technology. This tool employs a small oligonucleotide zipper that binds two miR-133a molecules via complementary interaction with their 5′ and 3′ ends. The zipper's nucleotides capture endogenous miRNA through complete complementary base pairing, although its sequence differs from miR-133a, with reversed 5′ and 3′ regions at either 11 nucleotides (11G11) or 14 nucleotides (14G8) from the 5′ end. Leveraging these features, we could inhibit miR-133a action with high affinity and specificity

by incorporating it into a template along with GFP siRNA, creating a bubble-like structure that self-assembles into an miR-133a zipper NP. This facilitates the delivery of the miRNA zipper into both monolayered adipocytes and adipose spheroids. This work showcases the potential of self-assembled miR-133a zipper NPs in delivering miR-133a zipper to adipocytes for therapeutic effects and for siRNA and the miRNA zipper co-delivery. Upon delivery into adipocytes, the miR-133a zipper is released, effectively binding endogenous miR-133a and promoting the expression of its target, *Prdm16*. We observed that treatment with the miR-133a zipper NP enhanced thermogenic gene expression and mitochondrial biogenesis in both monolayered adipocytes and adipose spheroids. In adipose spheroids, which more closely mimic in vivo conditions, we observed a reduction in adipose mass and an increase in cellular temperature following treatment with the miR-133a zipper NP. As the miR-133a zipper NP comprises only naturally biodegradable materials, our approach ensures biocompatibility and significantly reduces potential immune responses or other adverse effects associated with foreign materials such as LNPs, viruses, or inorganic substances.

Another important issue in gene therapy is tissue-specific targeting to prevent unintended physiological outcomes in non-pathogenic regions. miR-133a-mediated suppression of PRDM16 was selected as the target to introduce cell type specificity into the molecular mechanism of interaction with PRDM16. Studies show that direct PRDM16 overexpression can induce severe adverse effects derived from uncontrolled thermogenesis in other tissues and white fat depots. Experimentally, the injection of dinitrophenol (DNP), a classical mitochondrial uncoupling agent, causes heat production in all cells of the body, leading to uncontrolled hyperthermia.[57,58] Unlike this conventional method using artificial uncouplers, our approach represses the action of an endogenous Prdm16 inhibitor, miR-133a, thereby inducing thermogenesis only in adipose tissues or muscle where miR-133a mainly functions. MiR-133a inhibition has been shown to selectively induce PRDM16 overexpression in muscle and fat cells, making it an optimal selection for PRDM16 targeting.[57] With this approach, the thermogenic activity of the miR-133a inhibiting NP is limited to the innate action of miR-133a-mediated Prdm16 suppression, which occurs in fat and muscle cells, thus preventing excessive heat production in other tissue types and leading to off-target effects. Although miR-133a is mainly expressed in adipocytes, miR-133a zipper NPs could induce side effects when delivered to skeletal muscle or cardiac muscle, which could be further studied through in vivo testing. One previous literature generated miR-133a1$^{-/-}$a2$^{+/-}$ mice that have three out of the four miR-133a alleles knocked out, and those mice had normal cardiac and skeletal muscles, while the knock out resulted in browning of adipose tissues.[33] These findings introduce a novel RNAi platform that leverages a specially designed miR-133a zipper NP. In short, our developed platform holds great promise for anti-obesity treatments through the generation of thermogenic adipocytes. This technology has great potential for broader applications in various diseases, combining miRNA zipper technology with siRNA delivery for multifaceted therapeutic approaches. Overall, our innovative platform, leveraging meticulously designed self-assembled RNAi nanotechnology, not only holds great promise for anti-obesity treatments, but also has great potential for broader applications in various diseases that combine miRNA zipper technology with siRNA delivery for multifaceted therapeutic approaches.

4. Experimental Section

Preparation of cDNA Templates: A 5′-phophorylated linear DNA (PAGE purified, 85-base pair, 10 µM) was heated with a primer DNA containing T7 promoter sequence (22-base pair, 10 µM) in Duplex Buffer (30 mM HEPES, pH 7.5, 100 mM potassium acetate) (Integrated DNA Technologies, USA) at 95 °C for 2 min, then let cool down slowly to room temperature. After 1 h, the reaction vessel was added to the final concentration of 1X T4 buffer (50 mM Tris-HCl, 10 mM MgCl2, 1 mM ATP, 10 mM DTT, pH 7.5) (New England Biolabs, USA), 2.5 mM $MnCl_2$ (Sigma-Aldrich, USA), and 200 U µL^{-1} T4 DNA ligase (New England Biolabs, USA) to initiate the ligation of the nick DNA and form circularized DNA template. The ligation reaction was carried out at 16 °C for 18 h), and then the T4 DNA ligase was inactivated at 65 °C for 10 min. To remove linear free DNA from the reaction, the ligation reaction was diluted 1:10 and incubated with exonuclease 1 and 3 (New England Biolabs, USA) at 37 °C for 30 min. Subsequently, the reaction was stopped by adding EDTA to 11 mM, followed by heat inactivation at 80 °C for 30 min. The cDNA templates were used for subsequent steps without further purification.

The complete list of linear DNA and primer DNA sequences is presented in Table S1 (Supporting Information).

Oligonucleotides	Sequences (5′-3′)
T7 Primer	TAATACGACTCACTATAGGGAT
Template for miR-133a-Zipper 11G11	/5Phos/ATAGTGAGTCGTATTAAAGCAAGCTGACCC TGAAGTCAACCAGCTGCTTTGGTCCCCTGTGGA GCCTATTGCTTCGATTATCCCT
Template for complementary sequence of 11G11	/5Phos/ATAGTGAGTCGTATTAAATCGAAGCAATA GGCTCCACGTGTCATGAGACGGTCGAACCACC TTCAGGGTCAGCTTGCTTATCCCT
Template for miR-133a-Zipper 14G8	/5Phos/ATAGTGAGTCGTATTAAAGCAAGCTGACCC TGAAGACCAGCTGCTTTGGTCCCCTTCAGTGGA GCCTATTGCTTCGATTATCCCT
Template for complementary sequence of 14G8	/5Phos/ATAGTGAGTCGTATTAAATCGAAGCAATAG GCTCCACCACGTGTCATGAGACGGTCGAGTCTT CAGGGTCAGCTTGCTTATCCCT
FAM labeled Tag	/56-FAM/TCCCTATAGTGAGTCGTATT/3AmMO/

Synthesis of MiR-Zipper NPs: The miR-Zipper NPs were prepared by RCT using HiScribe T7 High Yield RNA Synthesis Kit (New England Biolabs, USA). To a 200 µL reaction, an equimolar amount of the two circularized DNA templates containing complementary sequences was added to the solution mixture containing T7 Reaction Buffer, ribonucleotides, and T7 RNA polymerase. The RCT reaction was conducted at 37 °C for 20 h. Then, the miR-Zipper NPs were purified by centrifugation and washed with nuclease-free water (QIAGEN, USA) 3 times and stored at 4 °C until further use. To fluorescently label miR-zipper NPs, 6-carboxyfluorescein (FAM)-labeled oligonucleotides (Integrated DNA Technologies, USA) containing complementary sequences to a non-functional portion of miR-zipper NPs were annealed to the particles at a final concentration of 10 µM at 65 °C for 10 min.

Analysis of Circularized DNA Templates by Agarose Gel Electrophoresis: The formation of circularized DNA templates was confirmed using agarose gel electrophoresis. Briefly, agarose gel was prepared by heating 1% agarose solution in Tris-acetate-EDTA (TAE) buffer, and then GelRed Nucleic Acid Gel Stain (Biotium) was added before gel solidified. The samples were mixed with 6X orange loading buffer (ThermoFisher Scientific, USA) prior to loading into the gel and electrophoresed at 90 V for 40–60 min. The gel images were visualized using a UV transilluminator (ThermoFisher Scientific, USA).

Characterization for NPs: For morphological characterization, a field emission scanning electron microscope (FE-SEM, Zeiss, Germany), a transmission electron microscopy (TEM, JEOL 1200EX electron microscope with AMT-XR41 digital camera, Japan), and an atomic force microscope (AFM, Park systems, NX10) were used to obtain morphology of the miR-Zipper NPs, while energy dispersive x-ray spectroscopy (FE-SEM with the EDS detector) was used for elemental composition. NP tracking analysis (NTA, NanoSight NS300, Malvern Panalytical Inc.) was used for size and number concentration characterization. The miR-Zipper NPs were sampled for FE-SEM and AFM by deposited on 10 mm V1 mica discs with 0.21 mm thickness (Ted Pella, Inc., USA, Cat. No. 50). For FE-SEM analysis, the air-dried samples were coated with gold (Au) before imaging. For AFM imaging, 10 µL of the reaction mixture was diluted in nuclease-free water containing 5 mM Tris-HCl and 5 mM MgCl2. After incubating the mixture at 4 ∘C for 30 min, 50 µL of the mixture was deposited onto the freshly cleaned mica surface, and further incubated at 4 ∘C for 30 min. Following the incubation, the mica surface was rinsed with deionized water to remove salts, and nitrogen gas was then sprayed onto the surface for three to five seconds to remove the remaining solution. The samples were scanned in non-contact mode with NC-NCH tips (Park Systems). For FE-SEM with EDS, 20 µL of the purified miRNA-133a zipper NPs were drop casted onto carbon tape and dried overnight in the desiccator. They were coated with platinum for SEM imaging and EDS analysis. For TEM analysis, the samples were deposited on carbon-coated copper (Cu) grids (Ted Pella Inc., USA), and then dried under vacuum before analysis. Hydrodynamic size of the NPs was measured on Malvern Instruments Zetasizer Nano ZS-90 (Malvern, USA).

SiRNA and MiR-Zipper Release from NP: To quantify the amount of siRNA and miR-Zipper molecules, a known number of miRNA-Zipper NPs measured using Nanodrop (ThermoFisher Scientific, USA) were incubated with recombinant dicer (Genlantis, USA) in a 10 µL reaction solution containing 1 µg of miR-Zipper NP, 1 mM ATP, 2.5 mM $MgCl_2$, 40% Dicer Reaction Buffer, 1U Recombinant Dicer Enzyme. The solution was incubated for different time periods (12 to 48 h) at 37 °C before adding Dicer Stop Solution to deactivate the Dicer enzyme. Generated siRNA molecules were then confirmed by gel electrophoresis with 3% agarose gel.

Quantification of SiRNA and MiR-Zipper Release: The generated miRNA-Zipper molecules were quantified using a stem-loop RT-qPCR method adopted from the literature to quantify small RNA.[59,60] The 11G11 and 14G8 miRNA-Zipper RNA molecules (Integrated DNA Technologies, USA) were used as standards for absolute quantification using SYBR Green Master Mix (ThermoFisher Scientific, USA) on a StepOnePlus real-time PCR System (Applied Biosystems, USA). All measurements were done in triplicate.

Native PAGE for Studying RNA Release from NP and RNA Binding: The same amount of target was incubated in nanopure water with each of sequences in increasing concentration at 60 °C for 20 min, followed by 20 min incubation at room temperature. Samples were prepared with gel loading buffer. To compare the binding efficiency of the NP and the target to other sequences, a 10% native PAGE was run at 10 V cm^{-2} for 2.5 h at 4 °C. The gel was stained and imaged. Quantification of band intensity was performed with the Thermo Fisher iBright imaging analysis software.

Cell Culture and Differentiation: 3T3-L1 preadipocyte cell line was purchased from ATCC (Cat. No. CL-173). The cells were grown in high-glucose Dulbecco's modified Eagle medium (DMEM, Welgene, Cat. No. LM001-05) supplemented with 10% bovine calf serum (BCS, Welgene, Cat. No. S103-01) and 1% penicillin/streptomycin (P/S, Welgene, Cat. No. LS202-02) at 37 °C in humidified 5% CO_2 incubator. For differentiation into mature adipocytes, 80% confluent 3T3-L1 cells were incubated in high-glucose DMEM with 10% fetal bovine serum (FBS, Welgene, Cat. No. S001-07), 1% P/S, 0.5 mM 3-isobutyl-1-methylxanthine (IBMX, Sigma, Cat. No. I5879), 1 µM dexamethasone (Sigma, Cat. No. D1756), and 10 µg mL^{-1} insulin (Sigma, Cat. No. I9278) for 2 days. Then, the cells were incubated in high-glucose DMEM with 10% FBS, 1% P/S, and 10 µg mL^{-1} insulin for further 6–8 days. The medium was changed every other day.

Adipose Spheroids Generation: Fully differentiated adipocytes in monolayer were detached from plates using Trypsin-EDTA solution. After dissociation, the cells were reaggregated in 96 well round bottom low adhesion plates (10 000 cells per well) in DMEM supplemented with 10% FBS and 1% P/S. 2 days after, adipose spheroids were transfected with miR-133a zipper or treated with RNA NP.

Transfection: Monolayered adipocytes or adipose spheroids were transfected with the original miR-133a zipper oligos (final 50 nM) using Lipofectamine 3000 reagent (Invitrogen, Cat. No. L3000001) according to the manufacturer's instruction. For monolayered adipocytes, transfection was performed twice for 4 days (once every two days). For adipose spheroids, transfection was performed three times for 6 days (once every two days). The sequences of miR-133a zipper oligos are as follow: 14G8, 5′-TGAAGGGACCAAAGCAGCTGGT-3′, 11G11, 5′-AGGGACCAAAGCAGCTGGTTGA-3′, LNA 11G11, 5′-A+GGGGACCAAAGCAGCTGGT+TGA-3′.

Analysis of RNA NP-Mediated GFP Knockdown: To evaluate the effects of siRNA targeting eGFP released from RNA NPs, differentiated adipocytes were transfected with pcDNA3-EGFP (Addgene, Cat. No. 13 031) using Lipofectamine 3000 reagent. After 6 h, the adipocytes were treated with miR-133a zipper NP (final concentration 20 µg mL^{-1}). 24 and 48 h after the treatment, the GFP signal was detected using Cytation 5 Cell Imaging Multi-Mode Reader (BioTek).

Reverse Transcription (RT)-Quantitative Polymerase Chain Reaction (qPCR): Total RNA was extracted from monolayered adipocytes or adipose spheroids using the Easy-Blue reagent (Intron, Cat. No. 17061). 1 µg of RNA was reverse transcribed into cDNA using the Maxime RT PreMix kit (Intron, Cat. No. 25081). qPCR was performed using KAPA SYBR FAST qPCR (Roche, Cat. No. KK4601) with a CFX96TM real-time PCR detector (Bio-Rad). Relative mRNA levels were normalized to β-actin or Gapdh mRNA levels for each target gene. The PCR primer sequences used are as follow: *Gapdh* forward, 5′- ATGACATCAAGAAGGTGGTG-3′, *Gapdh* reverse, 5′- CATACCAGGAAATGAGCTTG-3′, *Prdm16* forward, 5′-CAGCAC GGTGAAGCCATTC-3′, *Prdm16* reverse, 5′-GCGTGCATCCGCTTGTG-3′, *Ucp1* forward, 5′-ACTGCCACACCTCCAGTCATT-3′, *Ucp1* reverse, 5′-CTTTGCCTCACTCAGGATTGG-3′, *Fabp4* forward, 5′-AAGGTGAAGAGC ATCATAACCCT-3′, *Fabp4* reverse, 5′-TCACGCCTTTCATAACACATTCC-3′.

Quantification of MiRNA via RT-qPCR Analysis: The intracellular miRNA-133a level was quantified in each treatment condition from the total RNA extracted from culture using TRIZol reagent (Invitrogen, USA). The total RNA (100 ng) was subsequent to reverse transcription to form cDNA using miRCURY LNA RT kit (QIAGEN, USA). The cDNA was used as a template for real-time PCR analysis using miR-133a-specific assays in a miRCURY LNA miRNA PCR system (QIAGEN, USA), following the manufacturer's protocol, on a StepOnePlus real-time PCR System (Applied Biosystems, USA). The mmu-miR-133a-3p were used as miR-133a-specific primers and mmu-miR-103a-3p as the endogenous control. The two-step cycling conditions were performed as follows: Initiation activation at 95 °C for 2 min, 40 cycles of denaturation at 95 °C for 10 s, and combined annealing/extension at 56 °C for 60 s. The resulting CT values were normalized and reported in fold changes relative to the endogenous control (miR-103a-3p). All measurements were repeated three times.

Western Blot Assay: Protein lysates of adipocytes were extracted with Pro-prep reagent (Intron, Cat. No. 17081) for 1 min on ice and then centrifuged at 13,000 rpm at 4 °C for 20 min. The protein concentration of supernatants was measured using Bradford assay. 15 µg of proteins were subjected to sodium dodecyl sulfate-polyacrylamide gel electrophoresis (SDS-PAGE) (Figure S18, Supporting Information). Subsequently, the separated proteins were transferred onto polyvinylidene difluoride membranes (Millipore, Cat. No. IEVH00005) using a semi-dry transfer system (Bio-Rad). Then, the membranes were incubated with primary antibodies (Prdm16, Abcam, Cat. No. ab106410, Ucp1, Abcam, Cat. No. ab10983, α-tubulin, Santa Cruz, Cat. No. SC-32293) at 4 °C for 16 h on the shaker, followed by incubation with horseradish peroxidase (HRP)-conjugated secondary antibodies at room temperature for 1 h. The HRP signals were detected with chemiluminescence reagent (Absignal, Cat. No. ABC-3001) on AGFA 100 NIF X-ray film.

Mitochondrial Staining: Monolayered adipocytes or adipose spheroids were incubated with 200 nM of MitoTracker Green FM (Cell Signaling Technology, Cat. No. 9074) for 30 min at 37 °C. For staining the nucleus of adipocytes, Hoechst 33342 solution was also added with MitoTracker. Af-

ter incubation, the cells were washed with phosphate buffered saline (PBS) twice. The fluorescent signals of MitoTracker and Hoechst 33342 were detected using ZOE Fluorescent Cell Imager (Bio-Rad) or Cytation 5 Cell Imaging Multi-Mode Reader (BioTek). The signal intensities were quantified with ImageJ program.

Visualization of Thermogenesis: Adipose spheroids were incubated with 250 nM of ERthermAC temperature-sensitive live cell dye (Sigma-Aldrich, Cat. No. SCT057) in serum free medium for 30 min at 37 °C. After incubation, the cells were washed with PBS twice. The fluorescent signals were detected using Cytation 5 Cell Imaging Multi-Mode Reader (BioTek) and signal intensities were quantified with ImageJ program.

Statistical Analysis: Statistical significance was analyzed using one-way ANOVA with a post-hoc Tukey test or a two-way ANOVA with a post-hoc Tukey test where applicable and assessed based on *P* value. The number of values is listed for each analysis. All results with $*P < 0.05$, $**P < 0.01$, $***P < 0.001$, $****P < 0.0001$ were considered as statistically significant. The Statistical analysis was performed with Prism software version 10.1.0 (264).

Supporting Information

Supporting Information is available from the Wiley Online Library or from the author.

Acknowledgements

S.A.Y., T.P., and S.N. contributed equally to this work. Ki-Bum Lee acknowledges the partial financial support from the NSF (CBET-1803517), the New Jersey Commission on Spinal Cord (CSCR17IRG010, CSCR16ERG019), NIH R21 (R21-NS132556-01), and NIH R01 (1R01DC016612, 1R01NS130836-01A1, 3R01DC016612-01S1, and 5R01DC016612-02S1), NIH RM1 (RM1 NS133003-01), Alzheimer's Association (AARG-NTF-21-847862), CDMRP (OCRP, OC220235P1), N.J. Commission on Cancer Research (COCR23PPR007), and HealthAdvance (NHLBI, U01HL150852). S.A.Y. acknowledges financial support from the National Research Foundation of Korea (2017R1A6A3A04001986). T.P. acknowledges the NIH Postdoctoral Training for Translating Research in Regenerative Medicine (5T32EB005583). S.N. acknowledges fellowship support as part of the NIH T32 Biotechnology Training Program (GM135141). L.L.G. acknowledges fellowship support from the NSF GRFP (DGE-2233066). Some graphics in Figures 1, 2A, and 3A were created with BioRender.com.

Conflict of Interest

The authors declare no conflict of interest.

Data Availability Statement

The data that support the findings of this study are available from the corresponding author upon reasonable request.

Keywords

adipocyte browning, miRNA-133a zipper nanoparticles, RNA nanotechnology, RNAi therapeutics, thermogenic adipocytes

Received: February 20, 2024
Revised: May 17, 2024
Published online:

[1] J. K. Lam, M. Y. Chow, Y. Zhang, S. W. Leung, *Mol. Ther. Nucleic Acids* **2015**, *4*, E252.
[2] D. Peer, J. Lieberman, *Gene Ther.* **2011**, *18*, 1127.
[3] Y. K. Kim, *Exp. Mol. Med.* **2022**, *54*, 455.
[4] A. Curreri, D. Sankholkar, S. Mitragotri, Z. Zhao, *Bioeng. Transl. Med.* **2022**, *8*, e10374.
[5] K. Tatiparti, S. Sau, S. K. Kashaw, A. K. Iyer, *Nanomaterials* **2017**, *7*, 77.
[6] A. L. Jackson, J. Burchard, D. Leake, A. Reynolds, J. Schelter, J. Guo, J. M. Johnson, L. Lim, J. Karpilow, K. Nichols, W. Marshall, A. Khvorova, P. S. Linsley, *RNA* **2006**, *12*, 1197.
[7] P. Wang, Y. Zhou, A. M. Richards, *Theranostics* **2021**, *11*, 8771.
[8] S. Kauppinen, B. Vester, J. Wengel, *Drug Discov. Today Technol.* **2005**, *2*, 287.
[9] M. S. Ebert, J. R. Neilson, P. A. Sharp, *Nat. Methods* **2007**, *4*, 721.
[10] Z. Wang, *Methods Mol. Biol.* **2011**, *676*, 43.
[11] J. A. Kulkarni, D. Witzigmann, S. B. Thomson, S. Chen, B. R. Leavitt, P. R. Cullis, R. van der Meel, *Nat. Nanotechnol.* **2021**, *16*, 630.
[12] F. Borel, M. A. Kay, C. Mueller, *Mol. Ther.* **2014**, *22*, 692.
[13] G. Calcaterra, P. P. Bassareo, F. Barilla, F. Romeo, J. L. Mehta, *J. Cardiovasc. Med. (Hagerstown)* **2021**, *23*, 71.
[14] J. G. Rizk, A. Gupta, P. Sardar, B. M. Henry, J. C. Lewin, G. Lippi, C. J. Lavie, *JAMA Cardiol.* **2021**, *6*, 1451.
[15] A. Greinacher, K. Selleng, J. Mayerle, R. Palankar, J. Wesche, S. Reiche, A. Aebischer, T. E. Warkentin, M. Muenchhoff, J. C. Hellmuth, O. T. Keppler, D. Duerschmied, A. Lother, S. Rieg, M. P. Gawaz, K. A. L. Mueller, C. S. Scheer, M. Napp, K. Hahnenkamp, G. Lucchese, A. Vogelgesang, A. Flöel, P. Lovreglio, A. Stufano, R. Marschalek, T. Thiele, *Blood* **2021**, *138*, 1269.
[16] S. M. Moghimi, *Mol. Ther.* **2021**, *29*, 898.
[17] H. Jeon, S. Han, H. Kim, J. B. Lee, *J. Ind. Eng. Chem.* **2019**, *70*, 87.
[18] H. Kim, D. Kim, J. Jeong, H. Jeon, J. B. Lee, *Polymers (Basel)* **2018**, *10*, 589.
[19] M. Jang, J. H. Kim, H. Y. Nam, I. C. Kwon, H. J. Ahn, *Nat. Commun.* **2015**, *6*, 7930.
[20] J. B. Lee, J. Hong, D. K. Bonner, Z. Poon, P. T. Hammond, *Nat. Mater.* **2012**, *11*, 316.
[21] E. Kim, S. Agarwal, N. Kim, F. S. Hage, V. Leonardo, A. Gelmi, M. M. Stevens, *ACS Nano* **2019**, *13*, 2888.
[22] L. Meng, C. Liu, J. Lü, Q. Zhao, S. Deng, G. Wang, J. Qiao, C. Zhang, L. Zhen, Y. Lu, W. Li, Y. Zhang, R. G. Pestell, H. Fan, Y.i-H. Chen, Z. Liu, Z. Yu, *Nat. Commun.* **2017**, *8*, 13964.
[23] N. Arias, L. Aguirre, A. Fernández-Quintela, M. González, A. Lasa, J. Miranda, M. T. Macarulla, M. P. Portillo, *J. Physiol. Biochem.* **2016**, *72*, 509.
[24] M. Trajkovski, K. Ahmed, C. C. Esau, M. Stoffel, *Nat. Cell Biol.* **2012**, *14*, 1330.
[25] G. Solinas, J. Borén, A. G. Dulloo, *Mol. Metab.* **2015**, *4*, 367.
[26] S. Maurer, M. Harms, J. Boucher, *FEBS J.* **2021**, *288*, 3628.
[27] B. Cannon, J. Nedergaard, *Physiol. Rev.* **2004**, *84*, 277.
[28] P. Seale, B. Bjork, W. Yang, S. Kajimura, S. Chin, S. Kuang, A. Scimè, S. Devarakonda, H. M. Conroe, H. Erdjument-Bromage, P. Tempst, M. A. Rudnicki, D. R. Beier, B. M. Spiegelman, *Nature* **2008**, *454*, 961.
[29] S. Kajimura, P. Seale, K. Kubota, E. Lunsford, J. V. Frangioni, S. P. Gygi, B. M. Spiegelman, *Nature* **2009**, *460*, 1154.
[30] P. Seale, S. Kajimura, W. Yang, S. Chin, L. M. Rohas, M. Uldry, G. Tavernier, D. Langin, B. M. Spiegelman, *Cell Metab.* **2007**, *6*, 38.
[31] P. Seale, H. M. Conroe, J. Estall, S. Kajimura, A. Frontini, J. Ishibashi, P. Cohen, S. Cinti, B. M. Spiegelman, *J. Clin. Invest.* **2011**, *121*, 96.
[32] K. Ikeda, P. Maretich, S. Kajimura, *Trends Endocrinol. Metab.* **2018**, *29*, 191.
[33] W. Liu, P. Bi, T. Shan, X. Yang, H. Yin, Y. X. Wang, N. Liu, M. A. Rudnicki, S. Kuang, *PLoS Genet.* **2013**, *9*, e1003626.

[34] S. Kim, J. W. Park, M. G. Lee, K. H. Nam, J. H. Park, H. Oh, J. Lee, J. Han, S. A. Yi, J. W. Han, *J. Cell. Physiol.* **2019**, *234*, 3800.
[35] S. S. Choe, J. Y. Huh, I. J. Hwang, J. I. Kim, J. B. Kim, *Front. Endocrinol.* **2016**, *7*, 30.
[36] C. Hepler, R. K. Gupta, *Mol. Cell. Endocrinol.* **2017**, *445*, 95.
[37] S. Corvera, J. Solivan-Rivera, Z. Yang Loureiro, *Angiogenesis* **2022**, *25*, 439.
[38] C. M. Kusminski, P. E. Bickel, P. E. Scherer, *Nat. Rev. Drug Discov.* **2016**, *15*, 639.
[39] S. D. Rose, D. H. Kim, M. Amarzguioui, J. D. Heidel, M. A. Collingwood, M. E. Davis, J. J. Rossi, M. A. Behlke, *Nucleic Acids Res.* **2005**, *33*, 4140.
[40] S. A. Woodson, E. Koculi, *Methods Enzymol.* **2009**, *469*, 189.
[41] J. H. Lee, S. H. Ku, M. J. Kim, S. J. Lee, H. C. Kim, K. Kim, S. H. Kim, I. C. Kwon, *J. Controlled Release* **2017**, *263*, 29.
[42] H. Kim, J. Jeong, D. Kim, G. Kwak, S. H. Kim, J. B. Lee, *Adv. Sci.* **2017**, *4*, 1600523.
[43] D. Han, Y. Park, H. Kim, J. B. Lee, *Nat. Commun.* **2014**, *5*, 4367.
[44] D. Han, Y. Park, H. Nam, J. B. Lee, *Chem. Commun.* **2014**, *50*, 11665.
[45] M. H. Darvishi, A. Allahverdi, H. Hashemzadeh, H. R. Javadi, *Sci. Rep.* **2022**, *12*, 17520.
[46] J. Schauss, A. Kundu, B. P. Fingerhut, T. Elsaesser, *J. Phys. Chem. B* **2021**, *125*, 740.
[47] S. Chen, Q. Zhang, X. Wu, P. G. Schultz, S. Ding, *J. Am. Chem. Soc.* **2004**, *126*, 410.
[48] P. H. Hagedorn, R. Persson, E. D. Funder, N. Albæk, S. L. Diemer, D. J. Hansen, M. R. Møller, N. Papargyri, H. Christiansen, B.o R. Hansen, H. F. Hansen, M. A. Jensen, T. Koch, *Drug Discov. Today* **2018**, *23*, 101.
[49] T. C. Roberts, R. Langer, M. J. A Wood, *Nat. Rev. Drug Discov.* **2020**, *19*, 673.
[50] D. A. Braasch, D. R. Corey, *Chem. Biol.* **2001**, *8*, 1.
[51] J. Nedergaard, V. Golozoubova, A. Matthias, A. Asadi, A. Jacobsson, B. Cannon, *Biochim. Biophys. Acta* **2001**, *1504*, 82.
[52] M. Harms, P. Seale, *Nat. Med.* **2013**, *19*, 1252.
[53] A. J. Klingelhutz, F. A. Gourronc, A. Chaly, D. A. Wadkins, A. J. Burand, K. R. Markan, S. O. Idiga, M. Wu, M. J. Potthoff, J. A. Ankrum, *Sci. Rep.* **2018**, *8*, 523.
[54] A. D. Graham, R. Pandey, V. S. Tsancheva, A. Candeo, S. W. Botchway, A. J. Allan, L. Teboul, K. Madi, T. S. Babra, L. A. K. Zolkiewski, X. Xue, L. Bentley, J. Gannon, S. N. Olof, R. D. Cox, *Biofabrication* **2019**, *12*, 015018.
[55] A. Ioannidou, S. Alatar, R. Schipper, F. Baganha, M. Åhlander, A. Hornell, R. M. Fisher, C. E. Hagberg, *J. Physiol.* **2021**, *600*, 869.
[56] R. Sharma, S. Narum, S. Liu, Y. Dong, K. I. Baek, H. Jo, K. Salaita, *ACS Chem. Biol.* **2023**, *18*, 2349.
[57] J. Nedergaard, B. Cannon, *Cell Metab.* **2014**, *20*, 396.
[58] J. Grundlingh, P. I. Dargan, M. El-Zanfaly, *J. Med. Toxicol.* **2011**, *7*, 205.
[59] L. Tong, H. Xue, L. Xiong, J. Xiao, Y. Zhou, *Mol. Biotechnol.* **2015**, *57*, 939.
[60] C. Chen, *Nucleic Acids Res.* **2005**, *33*, e179.